# Crystal structure of brigatinib Form A (Alunbrig®), $C_{29}H_{39}ClN_7O_2P$

Ryan L. Hodge,[1] James A. Kaduk,[1,a)] Amy M. Gindhart,[2] and Thomas N. Blanton[2]
[1]*North Central College, 131 S. Loomis St., Naperville, Illinois 60540, USA*
[2]*ICDD, 12 Campus Blvd., Newtown Square, Pennsylvania 19073-3273, USA*

(Received 11 May 2021; accepted 15 August 2021)

The crystal structure of brigatinib Form A has been solved and refined using synchrotron X-ray powder diffraction data and optimized using density functional theory techniques. Brigatinib Form A crystallizes in space group *P*-1 (#2) with $a = 9.59616(20)$, $b = 10.9351(3)$, $c = 14.9913(6)$ Å, $\alpha = 76.1210(13)$, $\beta = 79.9082(11)$, $\gamma = 74.0802(6)°$, $V = 1458.497(15)$ Å$^3$, and $Z = 2$. Structure solution was complicated by the lowest cost factor solution having an unreasonable conformation of the dimethylphosphoryl group. The second-best structure yielded a better refinement. The crystal structure is characterized by alternating layers of aliphatic and aromatic portions of the molecules along the *b*-axis. Strong N–H···N hydrogen bonds link the molecules into pairs, with a graph set *R*2,2(8). There is a strong intramolecular N–H···O hydrogen bond to the phosphoryl group, which determines the orientation of this group. The powder pattern has been submitted to ICDD® for inclusion in the Powder Diffraction File™ (PDF®).  [doi:10.1017/S0885715621000518]

Key words: brigatinib, Alunbrig, Rietveld refinement, density functional theory

## I. INTRODUCTION

Brigatinib (Alunbrig®) is an anticancer drug specified as an anaplastic lymphoma kinase (ALK) inhibitor and tyrosine kinase inhibitor. It is mainly used as treatment in adult patients with metastatic ALK positive non-small cell lung cancer (NSCLC). Brigatinib targets a broad range of ALK mutations and ROS1 rearrangements (Camidge *et al.*, 2018). It is prescribed as a tablet and can be taken with or without food. The IUPAC name (CAS Registry number 1197953-54-0) is 5-chloro-4-*N*-(2-dimethylphosphorylphenyl)-2-*N*-[2-methoxy-4-[4-(4-methylpiperazin-1-yl)piperidin-1-yl]phenyl]pyrimidine-2,4-diamine. The molecular structure of brigatinib is illustrated in Figure 1.

Crystalline Forms A through H and J through K of brigatinib are claimed in International Patent Application WO 2016/065028 A1 (Rozamus, 2016; Ariad Pharmaceuticals Inc.) Single-phase powder X-ray diffraction (XRD) patterns are claimed for the eight forms A through H, and powder patterns for mixtures of Phase J and Phase A, and Phase K and Phase A are also presented. A small fraction of *d*-spacings for peaks observed in the powder XRD patterns are reported in WO 2016/065028, and there is no peak intensity data presented. Unit cell and refined crystal structure parameters collected at 150 K are provided for Form A, but no atomic coordinates are reported. Pharmaceutical compositions of brigatinib are claimed in International Patent Application WO 2019/158421 A1 (Martin, 2019; Sandoz), and powder diffraction data for Form A are provided as a comparative example.

This work was carried out as part of a project (Kaduk *et al.*, 2014) to determine the crystal structures of large-volume commercial pharmaceuticals, and include the atomic coordinates and high-quality powder diffraction data for these pharmaceuticals in the Powder Diffraction File (Gates-Rector and Blanton, 2019).

## II. EXPERIMENTAL

The sample was a commercial reagent, purchased from TargetMol (Lot #120474), and was used as-received. The light-yellow powder was packed into a 1.5 mm diameter Kapton capillary and rotated during the measurement at ~50 Hz. The powder pattern was measured at 295 K at beamline 11-BM (Lee *et al.*, 2008; Wang *et al.*, 2008) of the Advanced Photon Source at Argonne National Laboratory using a wavelength of 0.458119(2) Å from 0.5 to 50° 2$\theta$ with a step size of 0.001° and a counting time of 0.1 s per step.

The pattern was indexed on a primitive triclinic unit cell with $a = 9.95892$, $b = 10.93110$, $c = 14.97764$ Å, $\alpha = 76.18$, $\beta = 79.92$, $\gamma = 74.11°$, $V = 1457.61$ Å$^3$, and $Z = 2$ using JADE Pro (MDI, 2021). This is very close to the unit cell reported by Rozamus (2016), so the space group was assumed to be P-1. A reduced cell search in the Cambridge Structural

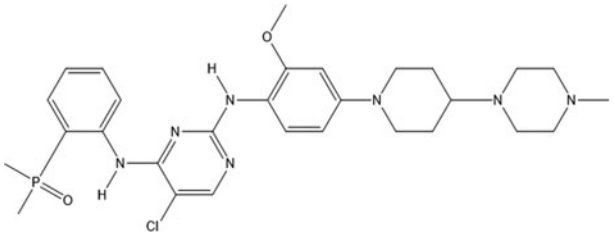

Figure 1. The 2D molecular structure of brigatinib.

a)Author to whom correspondence should be addressed. Electronic mail: kaduk@polycrystallography.com

 

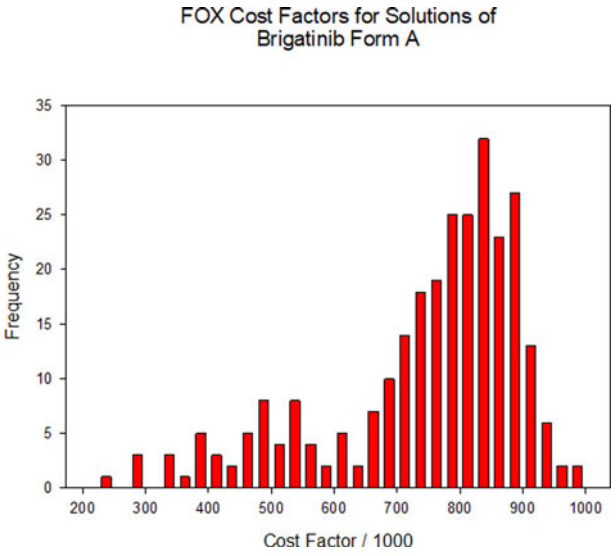


Figure 2. Distribution of the cost factors from 200 FOX structure solutions.

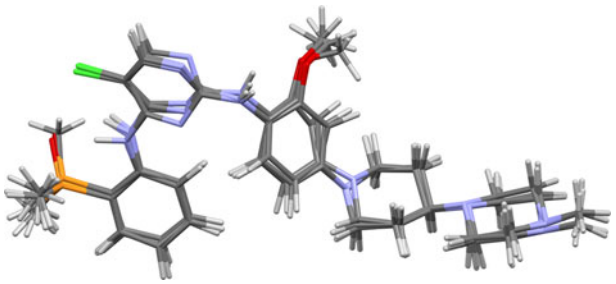

Figure 3. Overlay of the four best solutions from FOX. The lowest cost factor solution has a different orientation of the dimethylphosphoryl group than the next three.

Database (Groom *et al.*, 2016) yielded 1 hit, but no structures for brigatinib derivatives.

A brigatinib molecule was downloaded from PubChem (Kim *et al.*, 2019) as Conformer3D_CID_68165256.sdf. It was converted to a .mol2 fie using Mercury (Macrae *et al.*, 2020) and a Fenske–Hall *Z*-matrix using OpenBabel (O'Boyle *et al.*, 2011). The structural model was obtained by Monte Carlo simulated annealing techniques using FOX (Favre-Nicolin and Černý, 2002). Although most of the 200 solutions had cost factors in the range of 700 000 to 900 000 (Figure 2), the best solution had a cost factor of 242 861. The next three solutions (with cost factors of 276 992, 280 553, and 290 793) were also saved. Refinement of the best solution yielded $R_{wp} = 0.0781$. Although the four molecules from the four lowest cost factor solutions are generally similar (Figure 3), the lowest cost factor solution has a different conformation of the dimethylphosphoryl group. The other three solutions have the P=O oriented more reasonably, to form an intramolecular hydrogen bond to an N–H group (Figure 4). This "other" conformation (which yields a structure lower in energy by 1.5 kcal $mol^{-1}$) was used to begin the final refinement.

Rietveld refinement was carried out using GSAS-II (Toby and Von Dreele, 2013). Only the 1.5–25.0° portion of the pattern was included in the refinement ($d_{min} = 1.058$ Å). All non-H bond distances and angles were subjected to restraints, based on a Mercury/Mogul Geometry Check (Bruno *et al.*, 2004; Sykes *et al.*, 2011) of the molecule. The Mogul average and standard deviation for each quantity were used as the restraint parameters. The restraints contributed 9.6% to the final $\chi^2$. The hydrogen atoms were included in calculated positions, which were recalculated during the refinement using Materials Studio (Dassault, 2021). The $U_{iso}$ for the non-hydrogen atoms were grouped by chemical similarity. The $U_{iso}$ of the hydrogen atoms were constrained to be 1.3× that of the $U_{iso}$ of the heavy atoms to which they are attached. The background was modeled using a 4-term shifted Chebyshev polynomial, along with three peaks at 1.70, 5.72, and 22.20° to model the scattering from the Kapton capillary and the amorphous component of the sample. The peak profiles were described using the generalized microstrain model, and a spherical harmonic preferred orientation model was included.

The final refinement of 164 variables using 23 358 observations and 107 restraints yielded the residuals $R_{wp} = 0.0572$ and GOF = 1.39. The largest peak (2.26 Å from N5) and hole (1.69 Å from O4) in the difference Fourier map were 0.17 and −0.16(4) $e$Å$^{-3}$, respectively. The difference plot in

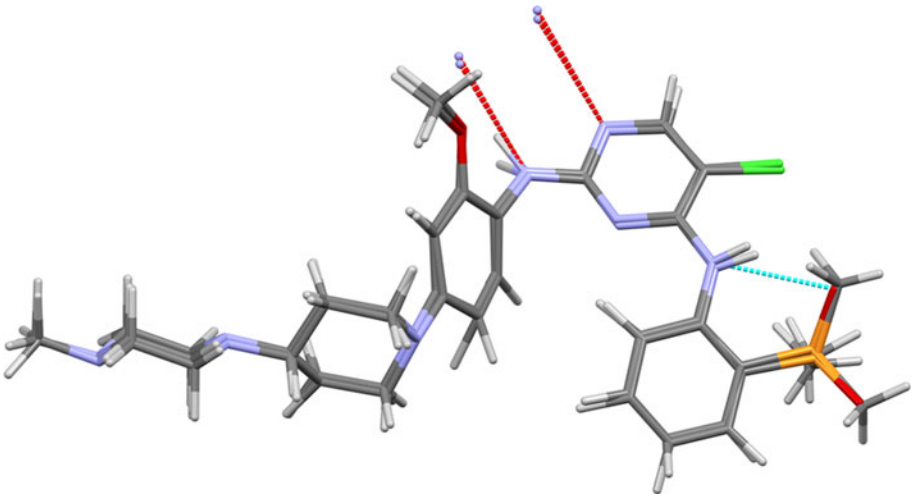

Figure 4. Overlay of the two best solutions, showing the additional intramolecular hydrogen bond in the second-best cost factor solution.


https://doi.org/10.1017/S0885715621000518 Published online by Cambridge University Press

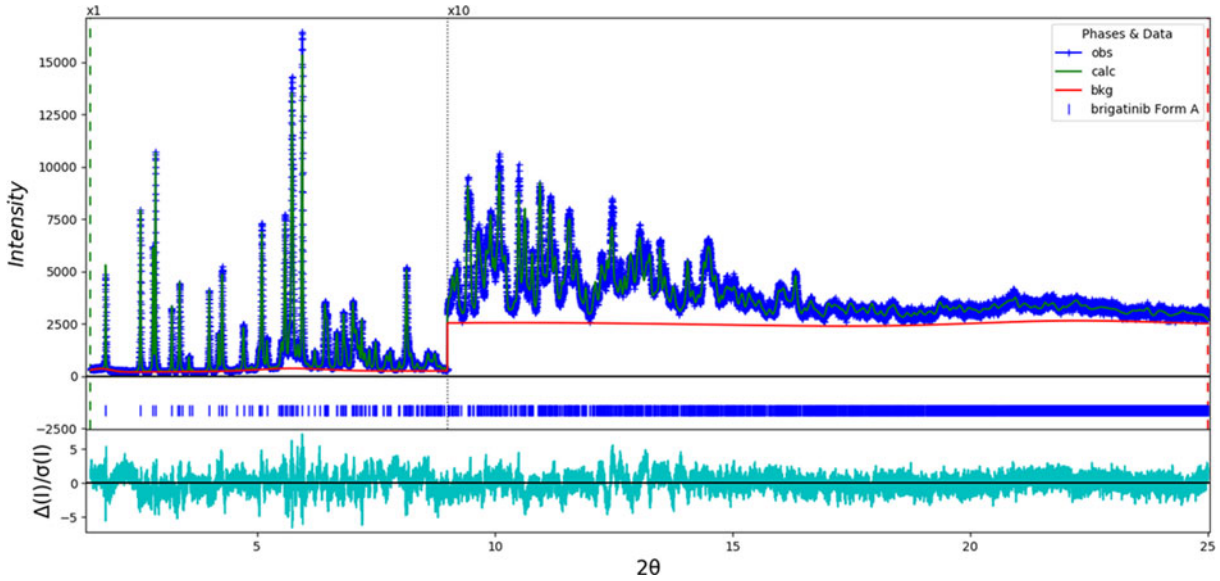


Figure 5. The Rietveld plot for the refinement of brigatinib Form A. The blue crosses represent the observed data points, and the Green line is the calculated pattern. The cyan curve is the normalized error plot. The vertical scale has been multiplied by a factor of 10× for $2\theta > 9.0°$.

the Rietveld-refined diffraction pattern (Figure 5) is quite flat; the largest errors are subtle ones in peak shape and/or intensity. A density functional geometry optimization (fixed experimental cell) and population analysis were carried out using CRYSTAL14 (Dovesi *et al.*, 2014). The basis sets for the H, C, N, and O atoms were those of Gatti *et al.* (1994), and the basis sets for P and Cl were those of Peintinger *et al.* (2013). The calculation was run on eight 2.1 GHz Xeon cores (each with 6 GB RAM) of a 304-core Dell Linux cluster at IIT, using 8 *k*-points and the B3LYP functional.

## III. RESULTS AND DISCUSSION

The synchrotron powder pattern of this study matches powder XRD patterns of Rozamus (2016) and Martin (2019) well enough (Figure 6) to conclude that all three samples represent brigatinib Form A. The refined atom coordinates of brigatinib Form A and the coordinates from the density functional theory (DFT) optimization are reported in the CIFs which have been deposited with ICDD. The root-mean-square (rms) Cartesian displacement of the non-hydrogen atoms in the Rietveld-refined and DFT-optimized

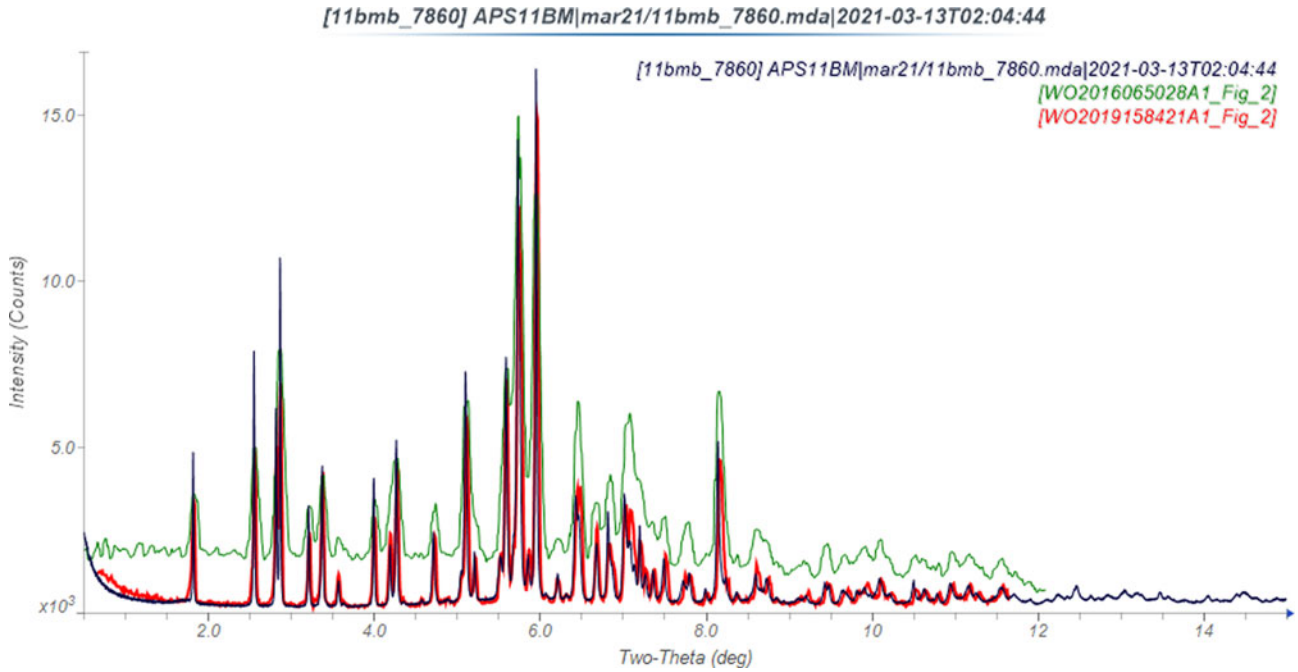


Figure 6. Comparison of the synchrotron pattern of brigatinib from this study to the patterns of Form A reported by Rozamus (2016) and Martin (2019). The published patterns were digitized using UN-SCAN-IT (Silk Scientific, 2013) and scaled to the synchrotron wavelength of 0.458119 Å using MDI JADE Pro (MDI, 2021).


https://doi.org/10.1017/S0885715621000518 Published online by Cambridge University Press

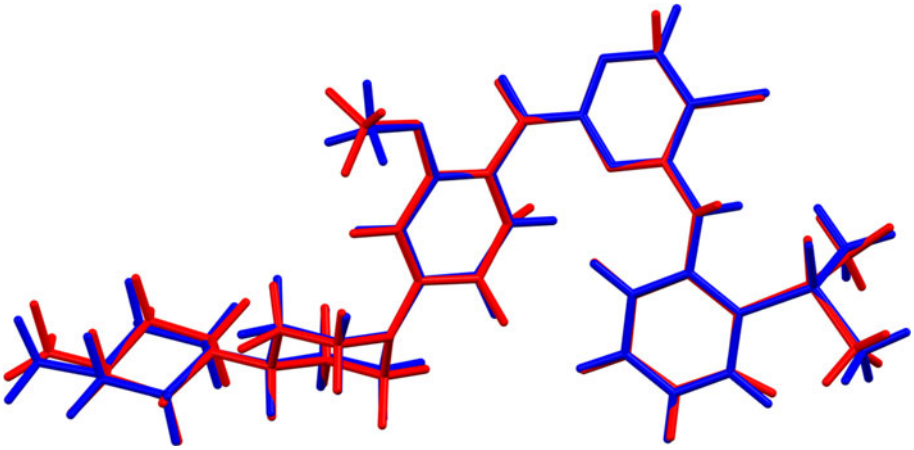

Figure 7. Comparison of the Rietveld-refined (red) and VASP-optimized (blue) structures of cation 1 of brigatinib Form A. The rms Cartesian displacement is 0.163 Å.

structures is 0.163 Å (Figure 7). The maximum displacement is 0.365 Å, at the methyl group C22. The excellent agreement is evidence that the structure is correct (van de Streek and Neumann, 2014). This discussion concentrates on the DFT-optimized structure. The asymmetric unit (with atom numbering) is illustrated in Figure 8, and the crystal structure is presented in Figure 9.

The crystal structure (Figure 9) is characterized by alternating layers of aliphatic and aromatic portions of the molecules along the *b*-axis. The molecular packing seems relatively loose along the *a*-axis. Most of the bond distances, angles, and torsion angles fall within the normal ranges indicated by a Mercury/Mogul Geometry check (Macrae *et al.*, 2020). The C32–C36–Cl1 angle of 122.0° is flagged as unusual (average = 119.9(7)°, *Z*-score = 3.2). The standard uncertainty on the average is very small, inflating the *Z*-score. The torsion angles involving rotation about the P2–C30 bond lie in broad distributions containing few hits, so it is hard to say if they are truly unusual. The C26–C27–N8–C28 torsion lies on the tail of the distribution of a small population. The torsion angles involving rotation about the C12–N5 bond lie outside of the usual *gauche/trans* distributions, and are truly unusual. These torsions involve rotation of the two saturated rings with respect to each other.

Quantum chemical geometry optimization of the brigatinib molecule (DFT/B3LYP/6-31G*/water) using Spartan '18 (Wavefunction, Inc., 2018) indicated that the observed solid-state conformation is 6.5 kcal $mol^{-1}$ higher in energy than the local minimum (Figure 10). The rms Cartesian displacement is 0.701 Å, and the differences in conformation are mainly in the orientation of the dimethylphosphoryl group and the saturated rings. The minimum energy conformation (Figure 11) is 3.5 kcal $mol^{-1}$ lower in energy. The rms Cartesian displacement is 1.403 Å, and the differences are spread throughout the molecule, particularly in the saturated rings. The differences show that solid-state interactions play a role in determining the observed conformation.

Analysis of the contributions to the total crystal energy using the Forcite module of Materials Studio (Dassault, 2021) suggests that angle distortion terms dominate the

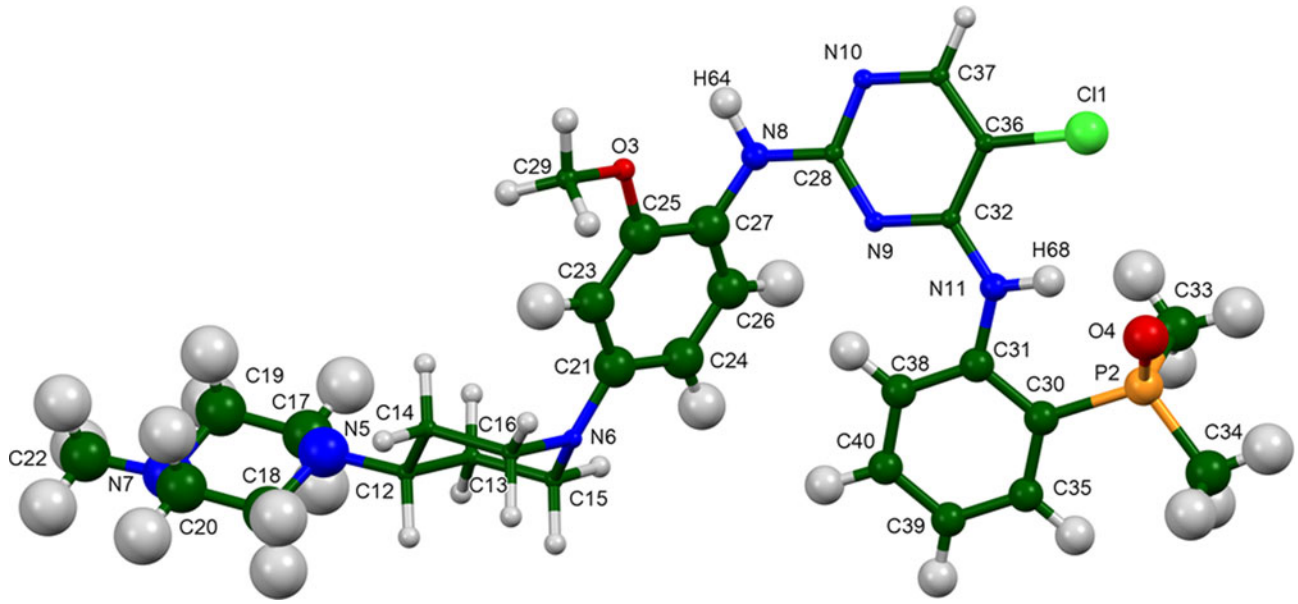


Figure 8. The asymmetric unit of brigatinib Form A, with the atom numbering. The atoms are represented by 50% probability spheroids.


https://doi.org/10.1017/S0885715621000518 Published online by Cambridge University Press

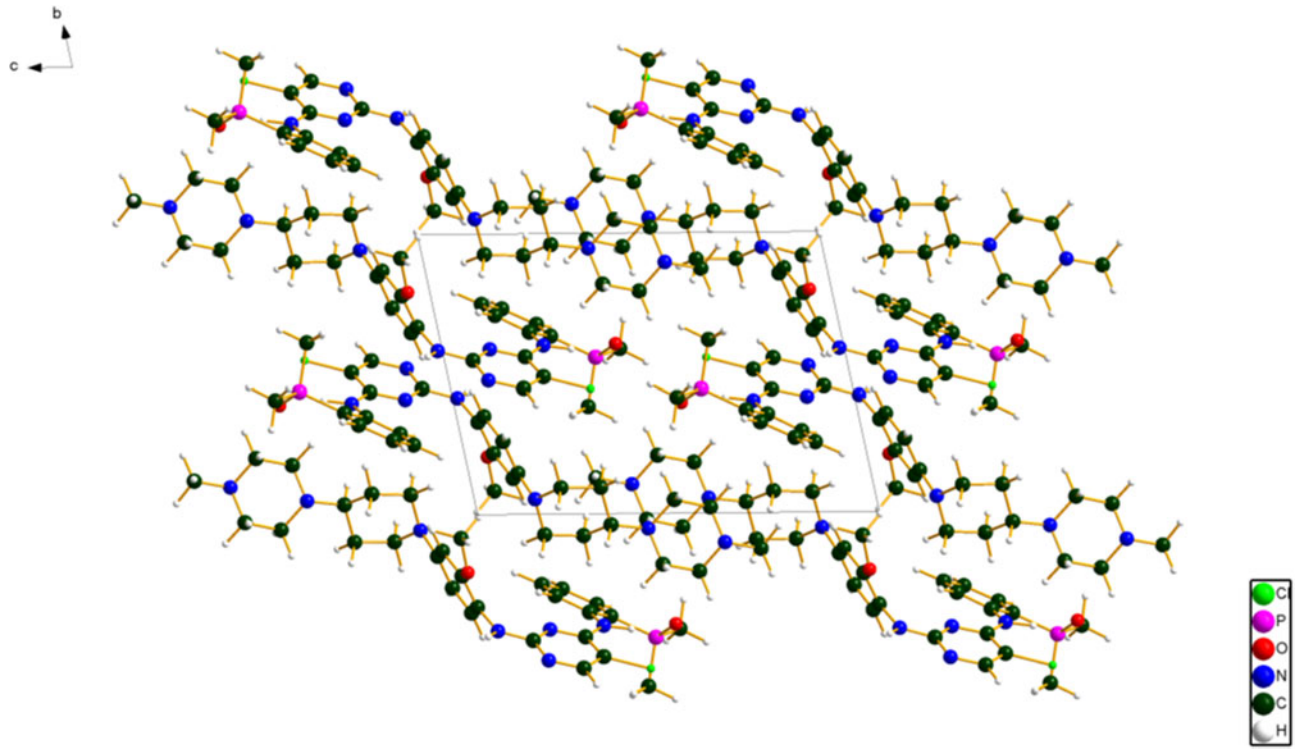


Figure 9. The crystal structure of brigatinib Form A, viewed down the *a*-axis.

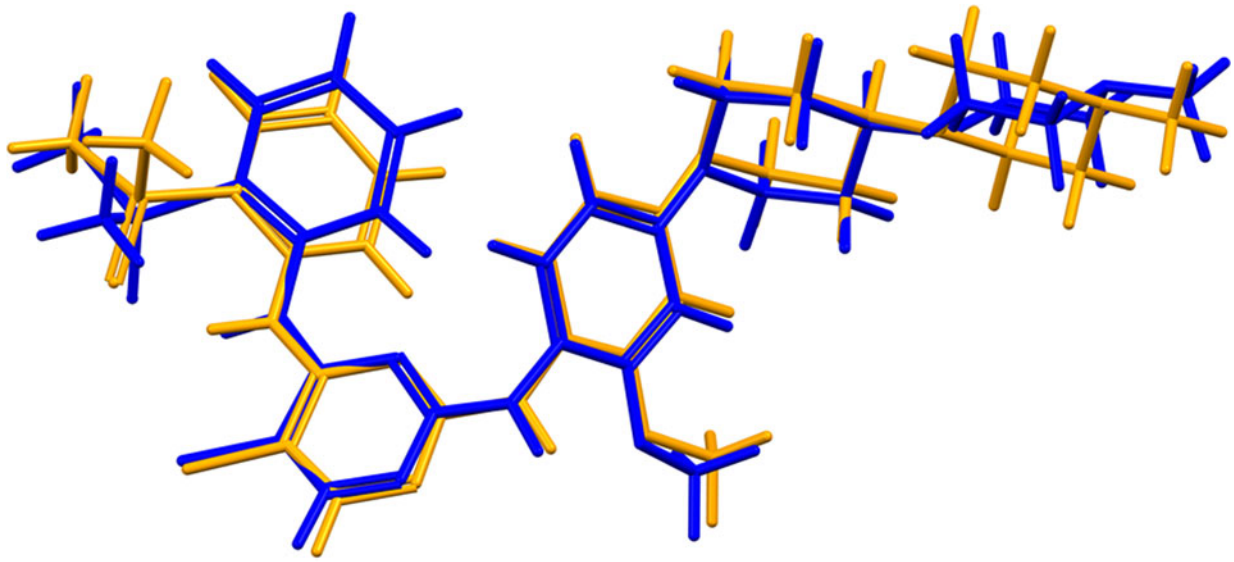


Figure 10. Comparison of the observed (blue) and DFT-optimized local minimum (orange) conformations of brigatinib in Form A.

intramolecular deformation energy. The intermolecular energy is dominated by electrostatic attractions, which in this force-field-based analysis include cation coordination and hydrogen bonds. The hydrogen bonds are better analyzed using the results of the DFT calculation.

Hydrogen bonds are significant in the crystal structure (Table I). Strong N8–H64···N10 hydrogen bonds link the molecules into pairs, with a graph set *R*2,2(8) (Etter, 1990; Bernstein *et al.*, 1995; Shields *et al.*, 2000). There is a strong intramolecular N11–H68···O4 hydrogen bond to the


https://doi.org/10.1017/S0885715621000518 Published online by Cambridge University Press

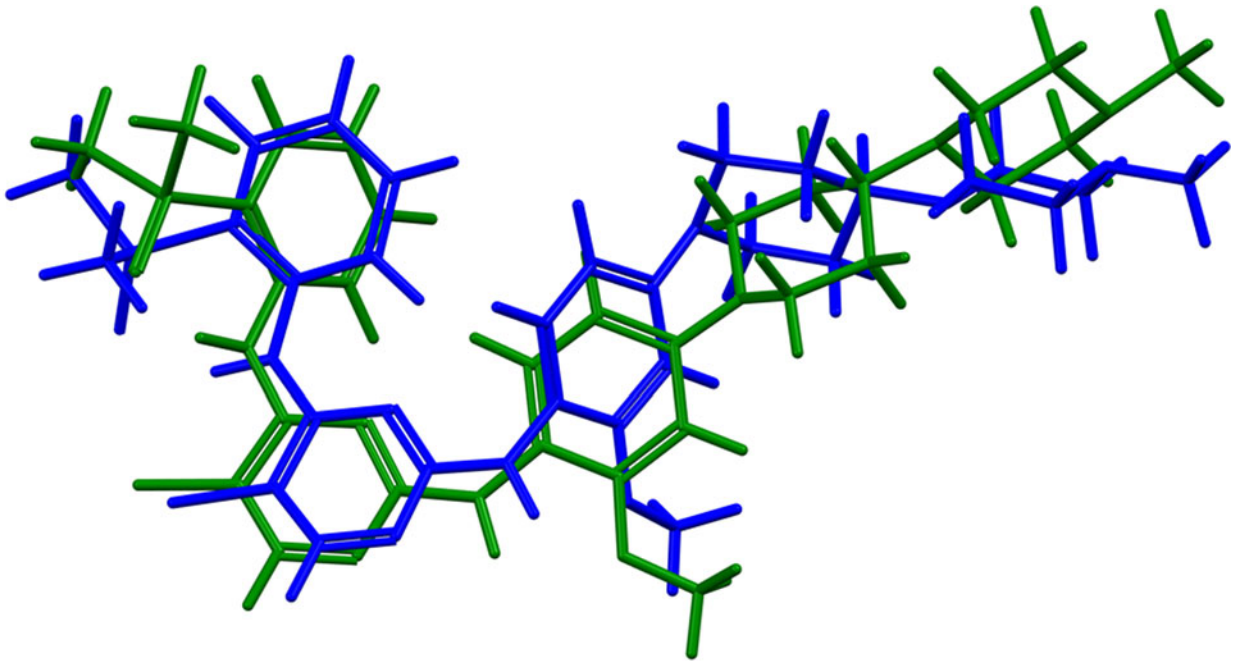


Figure 11. Comparison of the observed (blue) and global minimum-energy (Green) conformations of brigatinib in Form A.

TABLE I. Hydrogen bonds (CRYSTAL14) in brigatinib Form A

| H-Bond | D-H (Å) | H···A (Å) | D···A (Å) | D-H···A (°) | Overlap (*e*) | *E* (kcal mol$^{-1}$) |
|---|---|---|---|---|---|---|
| N8–H64···N10 | 1.028 | 1.987 | 3.013 | 176.6 | 0.062 | |
| N11–H68···O4 | 1.025 | 1.959[a] | 2.857 | 144.7 | 0.061 | 5.7 |
| C34–H73···O4 | 1.094 | 2.338 | 3.307 | 146.5 | 0.028 | |
| C33–H70···O4 | 1.094 | 2.510 | 3.419 | 139.8 | 0.018 | |
| N1–H68···Cl1 | 1.025 | 2.574[a] | 3.081 | 110.1 | 0.013 | |
| C34–H74···Cl1 | 1.093 | 3.104 | 4.156 | 161.8 | 0.010 | |
| C29–H66···N6 | 1.096 | 2.503 | 3.494 | 149.8 | 0.017 | |
| C38–H76···N9 | 1.078 | 2.215[a] | 2.880 | 117.8 | 0.010 | |
| H52···H41 | | 2.319[a] | | | 0.013 | |
| H55···H57 | | 2.502[a] | | | 0.012 | |
| H51-H52 | | 2.652[a] | | | 0.011 | |
| H57···H59 | | 2.575[a] | | | 0.010 | |
| H55···H59 | | 2.602[a] | | | 0.010 | |

[a]Intramolecular.

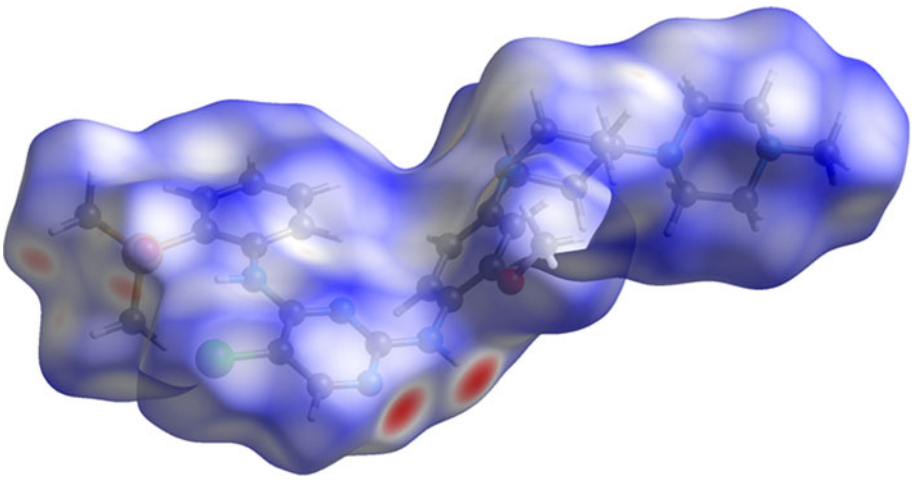

Figure 12. The Hirshfeld surface of brigatinib Form A. Intermolecular contacts longer than the sums of the van der Waals radii are colored blue, and contacts shorter than the sums of the radii are colored red. Contacts equal to the sums of radii are white.


https://doi.org/10.1017/S0885715621000518 Published online by Cambridge University Press

phosphoryl group, which determines the orientation of this group. The energy of this hydrogen bond was calculated using the correlation of Wheatley and Kaduk (2019). Several C–H···O, C–H···N, C–H···Cl, and N–H···Cl hydrogen bonds also contribute to the crystal energy. Several axial–axial and axial–methyl H···H interactions in the methylpiperazine ring seem to be significant.

The volume enclosed by the Hirshfeld surface (Figure 12; Hirshfeld, 1977; Turner *et al.*, 2017) is 719.15 Å$^3$, 98.62% of half the unit cell volume. The packing density is thus fairly typical. All of the significant close contacts (red in Figure 12) involve the hydrogen bonds. The volume/non-hydrogen atom is 18.2 Å$^3$.

The Bravais–Friedel–Donnay–Harker (Bravais, 1866; Friedel, 1907; Donnay and Harker, 1937) morphology suggests that we might expect platy morphology for brigatinib Form A, with {001} as the principal faces. A second-order spherical harmonic model for preferred orientation was incorporated into the refinement. The texture index was 1.031(0), indicating that preferred orientation was slight for this rotated capillary specimen. The powder pattern of brigatinib from this synchrotron data set has been submitted to ICDD for inclusion in the Powder Diffraction File™.

## IV. DEPOSITED DATA

The Crystallographic Information Framework (CIF) files containing the results of the Rietveld refinement (including the raw data) and the DFT geometry optimization were deposited with the ICDD. The data can be requested at info@icdd.com.


## ACKNOWLEDGEMENTS

The use of the Advanced Photon Source at Argonne National Laboratory was supported by the U.S. Department of Energy, Office of Science, Office of Basic Energy Sciences, under Contract No. DE-AC02-06CH11357. This work was partially supported by the International Centre for Diffraction Data. We thank Lynn Ribaud and Saul Lapidus for their assistance in the data collection, and Andrey Rogachev for the use of computing resources at Illinois Institute of Technology.


## CONFLICTS OF INTEREST

The authors have no conflicts of interest to declare.


Bernstein, J., Davis, R. E., Shimoni, L., and Chang, N. L. (**1995**). "Patterns in hydrogen bonding: functionality and graph set analysis in crystals," Angew. Chem. Int. Ed. **34**(15), 1555–1573 (in English).

Bravais, A. (**1866**). *Etudes Cristallographiques* (Gauthier Villars, Paris).

Bruno, I. J., Cole, J. C., Kessler, M., Luo, J., Motherwell, W. D. S., Purkis, L. H., Smith, B. R., Taylor, R., Cooper, R. I., Harris, S. E., and Orpen, A. G. (**2004**). "Retrieval of crystallographically-derived molecular geometry information," J. Chem. Inf. Sci. **44**, 2133–2144.

Camidge, D. R., Kim, H. R., Ahn, M. J., Yang, J. C. H., Han, J. Y., Lee, J. S., Hochmair, M. J., Li, J. Y. C., Chang, G. C., Lee, K. H., and Gridelli, C. (**2018**). "Brigatinib versus crizotinib in ALK-positive non-small-cell lung cancer," N. Engl. J. Med. **379**(21), 2027–2039.

Dassault Systèmes (**2021**). *Materials Studio 2021* (BIOVIA, San Diego, CA).

Donnay, J. D. H. and Harker, D. (**1937**). "A new law of crystal morphology extending the law of Bravais," Am. Mineral. **22**, 446–447.

Dovesi, R., Orlando, R., Erba, A., Zicovich-Wilson, C. M., Civalleri, B., Casassa, S., Maschio, L., Ferrabone, M., De La Pierre, M., D-Arco, P., Noël, Y., Causà, M., and Kirtman, B. (**2014**). "CRYSTAL14: a program for the ab initio investigation of crystalline solids," Int. J. Quantum Chem. **114**, 1287–1317.

Etter, M. C. (**1990**). "Encoding and decoding hydrogen-bond patterns of organic compounds," Acc. Chem. Res. **23**(4), 120–126.

Favre-Nicolin, V. and Černý, R. (**2002**). "FOX, free objects for crystallography: a modular approach to ab initio structure determination from powder diffraction," J. Appl. Crystallogr. **35**, 734–743.

Friedel, G. (**1907**). "Etudes sur la loi de Bravais," Bull. Soc. Fr. Mineral. **30**, 326–455.

Gates-Rector, S. and Blanton, T. N. (**2019**). "The Powder Diffraction File: a quality materials characterization database," Powder Diffr. **34**(4), 352–260.

Gatti, C., Saunders, V. R., and Roetti, C. (**1994**). "Crystal-field effects on the topological properties of the electron-density in molecular crystals - the case of urea," J. Chem. Phys. **101**, 10686–10696.

Groom, C. R., Bruno, I. J., Lightfoot, M. P., and Ward, S. C. (**2016**). "The Cambridge Structural Database," Acta Crystallogr. Sect. B: Struct. Sci., Cryst. Eng. Mater. **72**, 171–179.

Hirshfeld, F. L. (**1977**). "Bonded-atom fragments for describing molecular charge densities," Theor. Chem. Acta **44**, 129–138.

Kaduk, J. A., Crowder, C. E., Zhong, K., Fawcett, T. G., and Suchomel, M. R. (**2014**). "Crystal structure of atomoxetine hydrochloride (strattera), $C_{17}H_{22}NOCl$," Powder Diffr. **29**(3), 269–273.

Kim, S., Chen, J., Cheng, T., Gindulyte, A., He, J., He, S., Li, Q., Shoemaker, B. A., Thiessen, P. A., Yu, B., Zaslavsky, L., Zhang, J., and Bolton, E. E. (**2019**). "Pubchem in 2021: new data content and improved web interfaces," Nucleic Acids Res. **49**(D1), D1388–D1395. doi:10.1093/nar/gkaa971.

Lee, P. L., Shu, D., Ramanathan, M., Preissner, C., Wang, J., Beno, M. A., Von Dreele, R. B., Ribaud, L., Kurtz, C., Antao, S. M., Jiao, X., and Toby, B. H. (**2008**). "A twelve-analyzer detector system for high-resolution powder diffraction," J. Synchroton Radiat. **15**(5), 427–432.

Macrae, C. F., Sovago, I., Cottrell, S. J., Galek, P. T. A., McCabe, P., Pidcock, E., Platings, M., Shields, G. P., Stevens, J. S., Towler, M., and Wood, P. A. (**2020**). "*Mercury 4.0*; from visualization to design and prediction," J. Appl. Crystallogr. **53**, 226–235.

Martin, N. (**2019**). "Pharmaceutical composition of brigatinib," International Patent Application WO 2019/158421 A1.

MDI (**2021**). *JADE Pro Version 8.1 (Computer Software)* (Materials Data, Livermore, CA, USA).

O'Boyle, N., Banck, M., James, C. A., Morley, C., Vandermeersch, T., and Hutchison, G. R. (**2011**). "Open Babel: an open chemical toolbox," J. Chem. Informatics **3**, 33. doi:10.1186/1758-2946-3-33.

Peintinger, M. F., Vilela Oliveira, D., and Bredow, T. (**2013**). "Consistent Gaussian basis sets of triple-zeta valence with polarization quality for solid-state calculations," J. Comput. Chem. **34**, 451–459.

Rozamus, L. W. (**2016**). "Crystalline forms of 5-chloro-N4-[-2-(dimethylphosphoryl)phenyl]-N2-{2-methoxy-4-[4-(4-methylpiperazin-1-yl)piperidin-1-yl]pyrimidine-2,4-diamine," International Patent Application WO 2016/065028 A1.

Shields, G. P., Raithby, P. R., Allen, F. H., and Motherwell, W. S. (**2000**). "The assignment and validation of metal oxidation states in the Cambridge Structural Database," Acta Crystallogr. Sec. B: Struct. Sci. **56**(3), 455–465.

Silk Scientific (**2013**). *UN-SCAN-IT 7.0* (Silk Scientific Corporation, Orem, UT).

Sykes, R. A., McCabe, P., Allen, F. H., Battle, G. M., Bruno, I. J., and Wood, P. A. (**2011**). "New software for statistical analysis of Cambridge Structural Database data," J. Appl. Crystallogr. **44**, 882–886.

Toby, B. H. and Von Dreele, R. B. (**2013**). "GSAS II: the genesis of a modern open source all purpose crystallography software package," J. Appl. Crystallogr. **46**, 544–549.

Turner, M. J., McKinnon, J. J., Wolff, S. K., Grimwood, D. J., Spackman, P. R., Jayatilaka, D., and Spackman, M. A. (**2017**). *CrystalExplorer17* (University of Western Australia). Available at: http://hirshfeldsurface.net.

van de Streek, J. and Neumann, M. A. (**2014**). "Validation of molecular crystal structures from powder diffraction data with dispersion-corrected density functional theory (DFT-D)," Acta Crystallogr. Sect. B: Struct. Sci., Cryst. Eng. Mater. **70**(6), 1020–1032.

Wang, J., Toby, B. H., Lee, P. L., Ribaud, L., Antao, S. M., Kurtz, C., Ramanathan, M., Von Dreele, R. B., and Beno, M. A. (**2008**). "A dedicated powder diffraction beamline at the advanced photon source: commissioning and early operational results," Rev. Sci. Instrum. **79**, 085105.

Wavefunction, Inc. (**2018**). Spartan '18 Version 1.2.0, Wavefunction Inc., 18401 Von Karman Ave., Suite 370, Irvine, CA 92612.

Wheatley, A. M. and Kaduk, J. A. (**2019**). "Crystal structures of ammonium citrates," Powder Diffr. **34**, 35–43.



https://doi.org/10.1017/S0885715621000518 Published online by Cambridge University Press